

# Characterization of Thin and Ultrathin Polymer and Resist Films

Dario L. Goldfarb<sup>#</sup>, Qinghuang Lin<sup>#</sup>, Marie Angelopoulos<sup>#</sup>  
Christopher L. Soles<sup>\$</sup>, Eric K. Lin<sup>\$</sup>, and Wen-Li Wu<sup>\$</sup>

<sup>#</sup>IBM T. J. Watson Research Center, Route 134, Yorktown Heights, NY 10598.

<sup>\$</sup> Polymers Division, National Institute of Standards and Technology, Gaithersburg, MD 20899

## ABSTRACT

The need for a better understanding of the physicochemical properties of radiation-sensitive thin polymer coatings for lithographic applications is driven by the trend of ever-shrinking pattern dimensions and film thickness, imposed by the semiconductor industry. In this work, we address the issue of film uniformity and moisture absorption for thin and ultrathin films (250-50 nm) of poly 4-hydroxystyrene (PHS). Using high resolution x-ray reflectivity, the roughness and density of spin coated films was found to remain constant within experimental error for the thickness range examined. Also, water uptake on PHS films was studied by neutron and x-ray reflectivity. Exposure of the polymer film to a controlled humidity level is shown to swell the polymer and be absorbed uniformly throughout the film. No preferential absorption of water at the interface was noticed, regardless of the hydrophilic or hydrophobic nature of the substrate surface. Overall density changes in the polymer matrix due to the moisture-induced increase in the film thickness are also discussed.

**Keywords:** chemically amplified resists, ultra thin films, neutron reflectivity, x-ray reflectivity, poly 4-hydroxystyrene, roughness, density, moisture absorption.

## 1. INTRODUCTION

Optical solutions for future resist generations include 157 nm and EUV lithography. At these shorter wavelengths, virtually all the organic polymers presently used in photoresists are highly absorbing. This high absorbance renders traditional single layer imaging extremely difficult. Therefore, alternative lithography approaches have to be explored to accommodate the absorbance requirements. One alternative approach to the traditional single layer process is thin film imaging (TFI) where the image is first delineated in a thin imaging layer on top of an etch resistant and anti-reflective underlayer. The images thus defined are then transferred to an underlying underlayer through reactive ion etching (RIE). TFI includes bilayer, top surface imaging, thin resist coupled with a hard mask, as well as surface initiated growth imaging. It offers the benefits of a complete lithography and etch solution for device making. In a TFI scheme, the thin imaging layer provides resolution and process window and the underlayer offers etch resistance for image transfer to the substrates using RIE. The adoption of TFI for sub-100 nm device making will necessitate resist films with thickness substantially smaller than what has been practiced in the semiconductor industry (typically 500 nm to 1000 nm). At the 100 nm and 50 nm node, the resist thickness will approximately be 300 nm and 150 nm respectively based on the historical 3:1 aspect ratio irrespective of the exposure source (157 nm, EUV, projection e-beam (EPL), or direct write e-beam). When the optical absorbance issues are also taken into account, the resist thickness can drop to below 100nm. Therefore, thin (300 nm-100 nm) and ultrathin (sub-100nm) resists are likely to be needed for sub-100 nm patterning.

To date, very little work has been done to understand the film properties of resists below 300 nm. Below 100 nm substrate- and air-sample interfaces become critical. It can no longer be assumed that resists at this thickness will have the same properties and performance as that characteristic of thicker resists. These resist films can no longer be considered uniform and homogeneous films as in the traditional thick resist films. Surface confinement, substrate interactions and the resultant distribution of small molecules within the ultrathin films will dominate the properties and performance of the resists. Central to the investigation of structures and properties of ultrathin resist films are techniques capable of differentiating materials with high spatial resolution. Traditional techniques either generate average information of a resist film (such as FTIR, film thickness measurement techniques) or have limited spatial resolution (*e.g.* Rutherford backscattering spectroscopy, secondary ion mass spectroscopy). Therefore, techniques capable of characterizing ultrathin films with high spatial resolution are needed.

Recently, many efforts have been conducted to understand the behavior of ultrathin films by using high resolution reflectivity techniques. For example, x-ray (XR) and neutron (NR) reflectivity were used to characterize the effect of film thickness and substrate interactions on the thermal properties of thin films of polystyrene<sup>1,2</sup> and polymethylmethacrylate<sup>3,4</sup>. Dewetting as a probe of polymer mobility has been tested in thin films under confined geometries<sup>5</sup> and interdiffusion of miscible polymers over distances less than 20 nm has been reported<sup>6,7</sup>. The adsorption of water at a polyimide/silicon interface was previously studied using NR, providing the first quantitative evidence for a water concentration profile, which peaks in the interface region<sup>8</sup>.

In this work, we make use of XR to quantify the density and roughness as a function of thickness for thin and ultrathin films of poly 4-hydroxystyrene, a base resin for many 248 nm resists. Also, the extent of moisture uptake and the degree of swelling is evaluated using NR and XR, by exposing dry films of the same polymer to a well defined humidity level. Instead of using H<sub>2</sub>O, deuterium oxide (D<sub>2</sub>O) was chosen, since NR has the capability to capture the concentration profile of deuterated materials across a film of a complex polymer matrix, and provide information on concentration levels near a buried interface. The high contrast for neutrons exhibited by deuterium as compared to hydrogen is originated in a larger value of the elastic cohesive scattering length per unit volume ( $Q_c^2$ ).

## 2. EXPERIMENTAL

### 2.1 Materials and Sample Preparation

Solutions of poly 4-hydroxystyrene ( $M_w = 5000 \text{ g/mol}^{13}$ ) in propylene glycol methyl ether acetate (PGMEA) were prepared in concentrations or mass fractions of 3, 6, 8 and 10 %. Films of different thickness were formed by spin coating (Spin Headway Research<sup>14</sup>, 3000 rpm) the polymer solution on 3" and 4" silicon wafers featuring either HMDS (hydrophobic) or SiO<sub>x</sub> (hydrophilic) interfaces, followed by baking in a vacuum oven at 120 °C for 24 h. The film thickness ranged from 50 nm to 260 nm, analyzed by ellipsometry.

### 2.2 X-ray (XR) and Neutron (NR) Reflectivity

The detail of the reflectivity technique is displayed in Figure 1. In x-ray or neutron reflectivity, a monochromatic beam is incident at variable grazing incidence angles. The detector is set at the specular condition and the ratio of the reflected intensity vs the incident intensity is measured as a function of the momentum transfer normal to the surface ( $Q = (4\pi/\lambda)\sin\theta$ ), where  $\lambda$  is the x-ray wavelength and  $\theta$  is the angle of reflectance. A typical reflectivity profile from a thin uniform film of poly 4-hydroxystyrene (PHS) supported on a silicon wafer is shown in Figure 1. At very low  $Q$  values, total external reflection of the x-ray beam is observed. As  $Q$  increases, the reflectivity drops dramatically ( $Q_c$ ) when the x-ray beam begins to penetrate the sample surface. The periodic oscillations in the reflectivity profile result from constructive and destructive interference between the PHS/air interface and PHS/silicon interface. The reflectivity profile is sensitive to the widths of the interfaces and the structure of the film normal to the surface. In this plot, the large number of oscillations clearly indicates that the film has very little surface roughness. The linear profile of the film normal to the plane of the film can be determined by fitting the reflectivity data using a multiple layer matrix method. The XR technique is extremely sensitive to this profile and may be used to determine film thickness with a resolution of 0.1 nm, the density profile perpendicular to the plane of the film and the average roughness or quality of the film.

The specular neutron reflectivity measurements were performed at the National Institute of Standards and Technology Center for Neutron Research (NCNR) NG-7 reflectometer. The details of the experimental setup are reported elsewhere<sup>9</sup>. A thorough description of the x-ray reflectometer used in this study can be found in previous publications<sup>10,11</sup>.

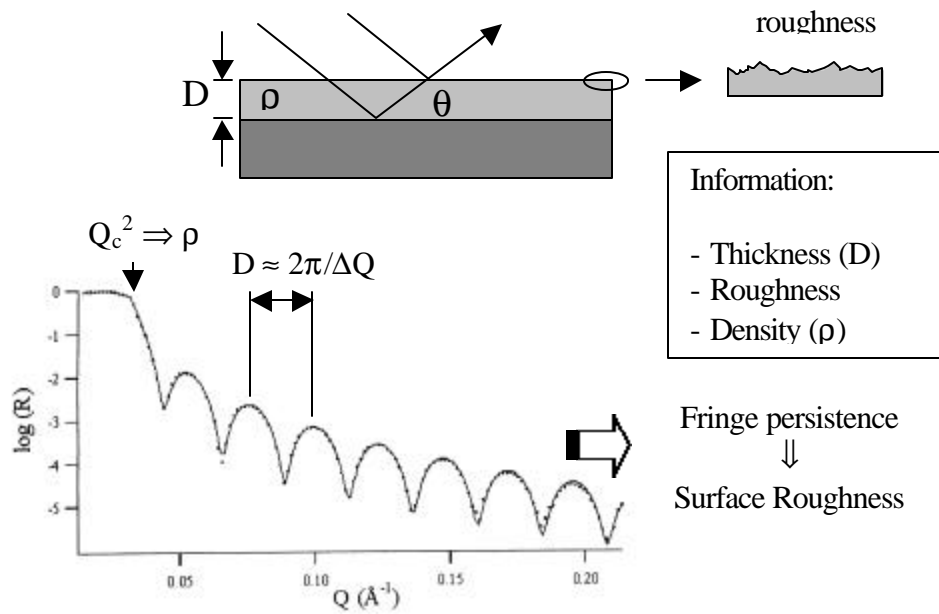


Figure 1. Basics of reflectivity ( $Q = 4\pi/\lambda \sin\theta$ )

### 3. RESULTS AND DISCUSSION

#### 3.1 Roughness and density of PHS samples as a function of film thickness from x-ray reflectivity (XR).

Figure 2 shows both the x-ray reflectivity data and the fits to the data for a PHS film on an HMDS-primed Si surface<sup>15</sup>. The data for each thickness is offset vertically for clarity. Tables 1 and 2 contain the thickness, XR roughness, and mass density (assuming the chemical composition of PHS) translated from the XR critical angle. It is noticeable that the roughness values for all of the PHS films are between (0.5 – 1.5) nm, independently of the nature of the interface (hydrophobic or hydrophilic). This variation does not show a systematic trend with the film thickness. Similar conclusions were obtained for an ESCAP-type resist by Okoroanyamwu<sup>12</sup> using both AFM and XR techniques.

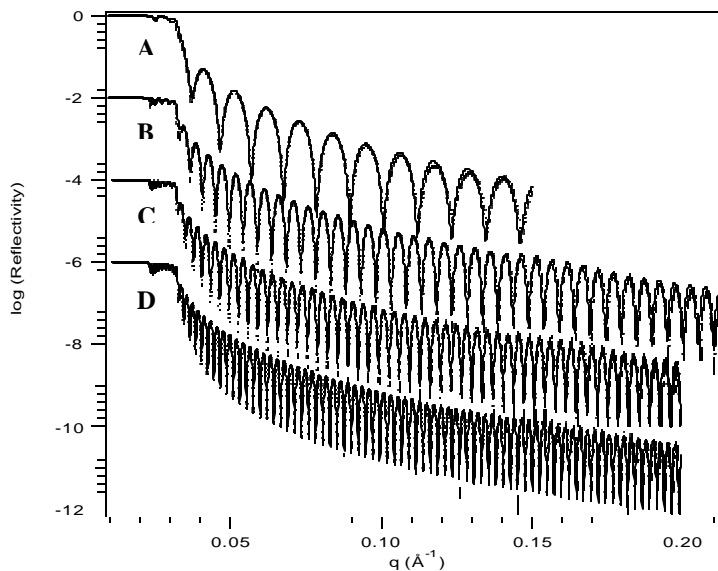


Figure 2. XR data (points) and fit to the data (solid lines) for poly 4-hydroxystyrene on an HMDS-primed Si surface. Thickness: A) 54.5 nm, B) 121.8 nm, C) 179.4 nm, D) 256.5 nm.

mass fraction	Thickness (nm)	XR roughness (nm)	Density (g/cm <sup>3</sup> )
3.0	54.5 ± 0.1	1.5 ± 0.5	1.20 ± 0.05
6.0	121.8 ± 0.1	1.0 ± 0.3	1.18 ± 0.05
8.0	179.4 ± 0.1	0.5 ± 0.2	1.18 ± 0.05
10.0	256.5 ± 0.1	0.5 ± 0.2	1.18 ± 0.05

Table 1. Thickness, XR roughness, and mass density for poly 4–hydroxystyrene on an HMDS-primed Si surface, as obtained from the experimental data shown in Figure 2.

mass fraction	Thickness (nm)	XR roughness (nm)	Density (g/cm <sup>3</sup> )
3.0	54.2 ± 0.1	0.5 ± 0.2	1.19 ± 0.05
6.0	123.2 ± 0.1	0.5 ± 0.2	1.18 ± 0.05
8.0	178.3 ± 0.1	1.0 ± 0.3	1.18 ± 0.05
10.0	259.8 ± 0.1	1.0 ± 0.3	1.18 ± 0.05

Table 2. Thickness, XR roughness, and mass density for poly 4–hydroxystyrene on a native SiO<sub>x</sub> surface, as obtained from experimental data (not shown).

### 3.2 PHS Thin Film Moisture Absorption

PHS films with thickness values ranging from approximately 500 Å to 2500 Å were spun coat onto Si wafers with either a SiO<sub>x</sub> (hydrophilic) or HMDS (hydrophobic) surface treatment. The moisture absorption was observed *in situ* using neutron and X-ray reflectivity. The films were first characterized under vacuum, after which they were exposed to a D<sub>2</sub>O partial pressure of approximately 2240 Pa. After approximately 1 h of exposure to the D<sub>2</sub>O vapor, the second reflectivity curve was obtained. The reflectivity curves were then fit to extract the film thickness and density profile normal to the film surface. Figure 3 demonstrates a typical set of wet and dry X-ray reflectivity curves for the thinnest films, with the real space density profiles (in units of Q<sub>c</sub><sup>2</sup>) shown in Figure 4.

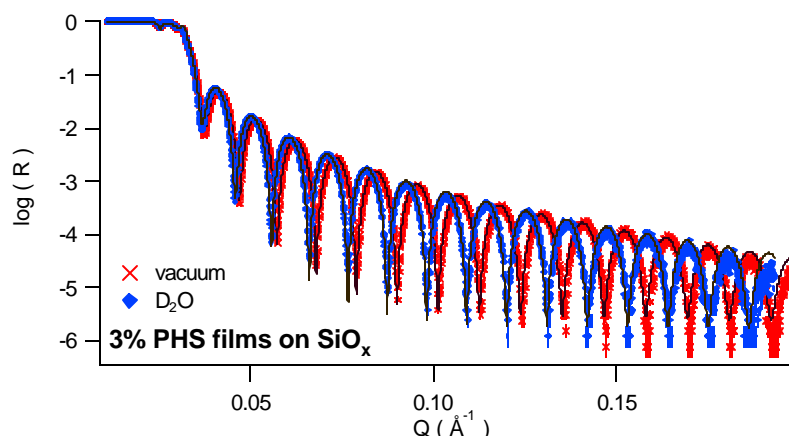


Figure 3. X-ray reflectivity from the 3.0 % PHS films on SiO<sub>x</sub>.

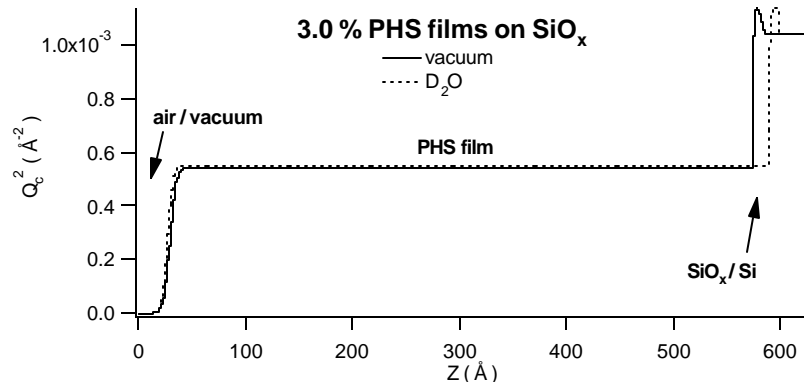


Figure 4. Real-space X-ray density profiles from the 3.0 % PHS films on SiO<sub>x</sub>.

With the exception of the different scattering length densities, the neutron reflectivity results from the same films in Figures 5 and 6 are consistent with the X-ray data, as displayed in Figures 3 and 4.

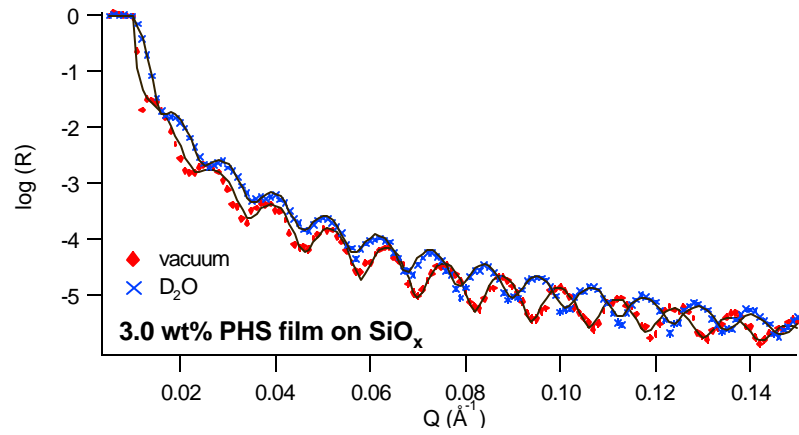


Figure 5. Neutron reflectivity from the 3.0 % PHS films on SiO<sub>x</sub>.

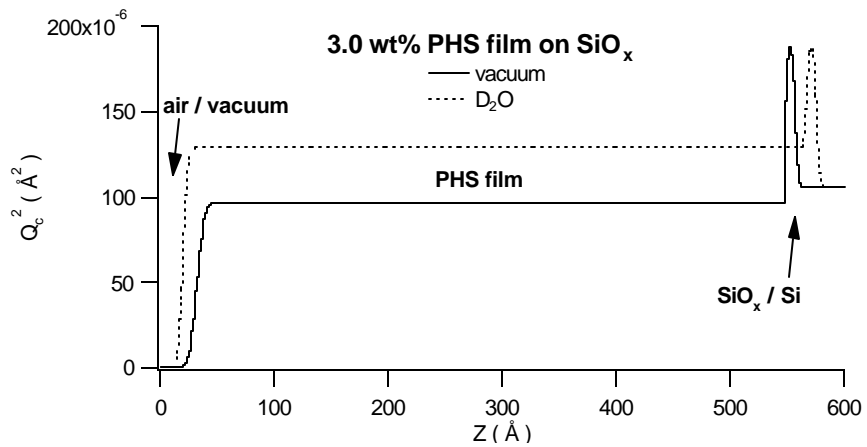


Figure 6. Real-space neutron density profiles from the 3.0 % PHS films on SiO<sub>x</sub>.

The most notable observation from Figures 3 through 6 is that the PHS film, whether swollen with D<sub>2</sub>O or dry, is modeled as a single layer of uniform density. D<sub>2</sub>O has a very strong contrast with the PHS in neutron reflectivity ( $Q_c^2 = 428 \times 10^{-6} \text{ \AA}^{-2}$  for pure D<sub>2</sub>O vs.  $87 \times 10^{-6} \text{ \AA}^{-2}$  for PHS), and preferential absorption at the interface would readily show up in Figures 5 and 6. Such a preferential absorption has been observed in polyimide films<sup>8</sup> and is anticipated in many epoxy/glass fiber (which also have SiO<sub>x</sub> surfaces) composites. In Figure 6 it is also interesting to note that neutron reflectivity indicates a significant increase in density of the D<sub>2</sub>O soaked PHS films while the X-ray reflectivity (Figure 4) does not. This is primarily an isotopic effect when -OD from the D<sub>2</sub>O exchanges with -OH from the PHS.

A very analogous behavior is observed with the thickest PHS films. Figures 7 and 8 display the X-ray reflectivity curves and real space profiles for the approximately 2500 Å PHS films supported on SiO<sub>x</sub>.

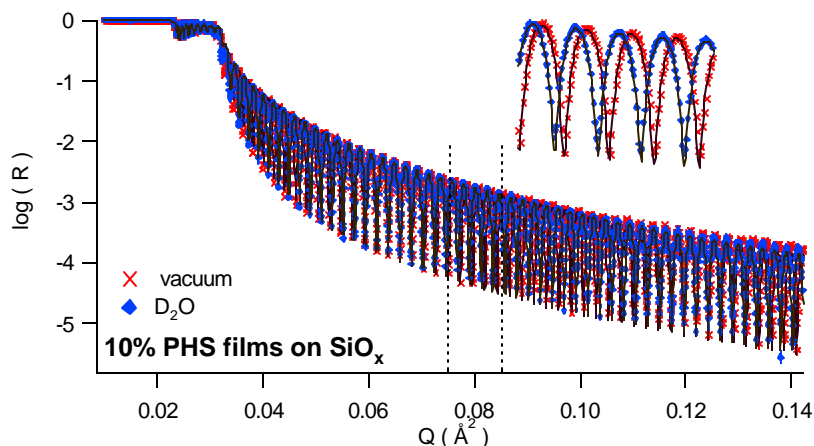


Figure 7. X-ray reflectivity from the 10.0 % PHS films on SiO<sub>x</sub>.

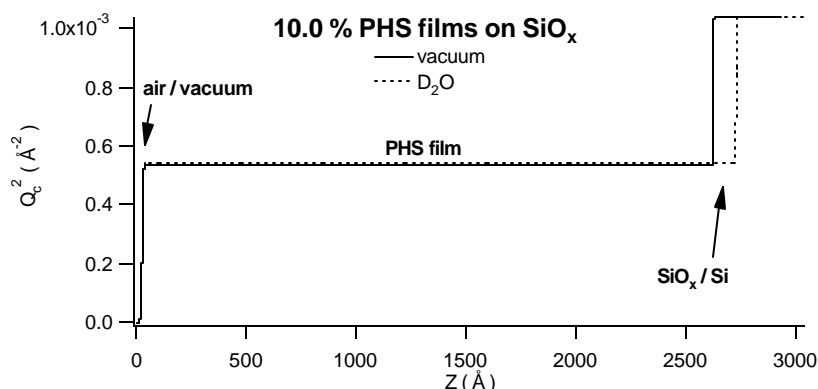


Figure 8. Real-space X-ray density profiles from the 10.0 % PHS films on SiO<sub>x</sub>.

While the interference fringes are more tightly spaced because of the increased film thickness, the same general behavior is observed as with the thinner films; the polymeric layer appears to be of uniform density in both the wet and dry states. However, Figures 7 and 8 are from X-ray reflectivity where there is not a strong contrast between the water and the PHS; standing alone, Figures 7 and 8 would not provide conclusive evidence of a uniform film density. Neutron reflectivity is really needed to determine if D<sub>2</sub>O segregation occurs. Unfortunately the films on the order of 2500 Å are too thick to resolve with our neutron reflectometer. This prohibits us from seeing interference fringes and makes it extremely difficult to extract reliable thickness and density profile information from simple curves fitting alone.

However, we can ascertain that significant D<sub>2</sub>O segregation does not occur in these thicker films by modeling the smooth neutron reflectivity curves. Using the wet film thickness obtained from the X-ray reflectivity (2703.8 Å) in Figure 7 and the

$Q_c^2$  obtained from the neutron reflectivity on the thinner wet film presented in Figure 6 ( $129 \times 10^{-6} \text{ \AA}^{-2}$ ), the modeled neutron reflectivity for the wet 10% PHS on  $\text{SiO}_x$  sample does an excellent job parameterizing the experimental data, as presented in Figure 9.

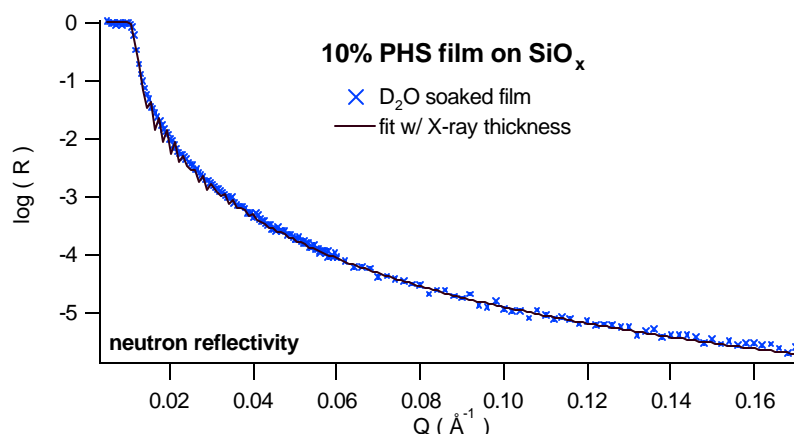


Figure 9. Neutron reflectivity from the 10% PHS on  $\text{SiO}_x$  soaked in  $\text{D}_2\text{O}$ . The solid line parameterizing the data is described above in the text.

Despite the lack of interference fringes, the fact that the modeled reflectivity curve captures the  $Q$  dependence of the reflected intensity is very strong evidence that the single layer model with uniform  $\text{D}_2\text{O}$  absorption is correct; preferential interfacial absorption does not occur in either the thin or thick PHS films.

All of the reflectivity curves presented thus far have been for the  $\text{SiO}_x$  substrate. Although they are not shown here, identical trends are observed on the HMDS treated silicon substrates.

Up to this point, we have not addressed the magnitude of the film density changes or the degree of swelling in the films. These values are tabulated for the PHS films on the two different substrates in Table 3. The most striking feature in Table 3 is the discrepancy between the swellings observed with neutrons in comparison to X-rays. The neutron-based measurements indicate a moisture-induced thickness expansion of 6 % to 8 % in contrast to approximately 3 % to 4 % for the X-rays. However, this difference is primarily an artifact of the non-reversible nature of the initial moisture uptake. After spin coating, the excess solvent was removed by baking the films at  $120^\circ\text{C}$ . The first measurements were then made under vacuum, and then under  $\text{D}_2\text{O}$  vapor, using neutron reflectivity. For example, in the 3.0% PHS film on  $\text{SiO}_x$ , the resulting dry and wet thickness values were  $515.7 \text{ \AA}$  and  $546.7 \text{ \AA}$  respectively, corresponding to 6.0 % linear swelling. However, when this film was redried and measured with neutron reflectivity again the vacuum thickness was  $524.8 \text{ \AA}$ , approximately 4.2 % of contraction from the wet thickness. This contraction of 4.2 % in neutrons is consistent with the X-ray measurements and we therefore conclude that the seemingly excessive expansion in the neutron reflectivity is attributed to the non-reversible nature of the initial  $\text{D}_2\text{O}$  uptake.

Table 3 also reports the changes in the critical angle for total reflection ( $Q_c^2$ ) which is directly proportional to the overall density in the absence of exchange interactions. With regards to the neutron measurements, the isotopic effect of replacing  $-\text{OH}$  with  $-\text{OD}$  in PHS results in a 34.5 % increase in  $Q_c^2$  in the absence of a density change. From the changes in  $Q_c^2$  reported in Table 3 is apparent that such an exchange occurs. Furthermore, for the initial vacuum,  $\text{D}_2\text{O}$  soaked, and redried experiments discussed above with the non-reversibility, the corresponding  $Q_c^2$  values were  $96.9 \times 10^{-6} \text{ \AA}^{-2}$ ,  $129 \times 10^{-6} \text{ \AA}^{-2}$ , and  $114 \times 10^{-6} \text{ \AA}^{-2}$  respectively, indicating that some  $-\text{OD}$  remains in the PHS after drying. If one assumes that all of the  $-\text{OH}$ s in PHS are replaced with  $-\text{OD}$ s, one can take into account the isotopic effect, as shown in Table 3. The results show a net increase in the scattering length density of the 3.0 % PHS on  $\text{SiO}_x$  and a decrease on the HMDS substrate. However, the magnitude of these changes is comparable with the typical  $\pm 5\%$  error in our ability to determine density from a  $Q_c^2$  measurement and we refrain from interpreting density changes in the neutron data. The possibility of incomplete or partial deuterium exchange makes density inferences from the neutron data even more suspect.

		3% PHS SiOx	3% PHS HMDS	10% PHS SiOx	10% PHS HMDS
NR	Vac thickness (Å)	515.70	519.10		
	D <sub>2</sub> O thickness (Å)	546.70	560.80	Too thick to quantify	
	% swelling	6.0%	8.0%		
	vac Q <sub>c</sub> <sup>2</sup> (Å <sup>-2</sup> )	9.69E-05	9.86E-05		
	D <sub>2</sub> O Q <sub>c</sub> <sup>2</sup> (Å <sup>-2</sup> )	1.29E-04	1.37E-04	Too thick to quantify	
	% change	24.9%	39.0%		
	% change*	-9.6%	4.5%		
XR	vac thickness (Å)	542.00	545.30	2598.20	2565.10
	D <sub>2</sub> O thickness (Å)	560.30	567.90	2703.80	2652.20
	% swelling	3.4%	4.1%	4.1%	3.4%
	vacuum Q <sub>c</sub> <sup>2</sup> (Å <sup>-2</sup> )	5.40E-04	5.41E-04	5.35E-04	5.34E-04
	D <sub>2</sub> O Q <sub>c</sub> <sup>2</sup> (Å <sup>-2</sup> )	5.46E-04	5.46E-04	5.44E-04	5.43E-04
	% change	1.1%	0.9%	1.7%	1.7%
	* normalized for isotopic effect; -OH to -OD in PHS increases Q <sub>c</sub> <sup>2</sup> by 34.5%				

Table 3. Wet and dry PHS film thickness values and scattering length densities (Q<sub>c</sub><sup>2</sup>).

With X-ray reflectivity, the -OH to -OD exchange effect on the measured signal is negligible and we note that there appears to be a systematic change in Q<sub>c</sub><sup>2</sup> between the thin and thick PHS films in Table 3. In the thin (3.0 %) films, Q<sub>c</sub><sup>2</sup> increases by 0.9 % to 1.1% upon D<sub>2</sub>O absorption versus 1.7 % in the thicker analogs, regardless of surface energy. While the differences are smaller than our typical errors, the trends are consistent; the thinner films appear to densify less than the thicker films. Looking at the values of Q<sub>c</sub><sup>2</sup>, the vacuum values are greater in the thinnest films, suggesting that the thinner films are slightly denser. This observation is extremely intriguing in light of the fact that thinner resist films (on the order of 1000 Å) show both a decreased image quality as well as an increased reactive ion etch resistance. In this respect, it might be worthwhile to further investigate this notion in a more focused set of experiments.

#### 4. SUMMARY AND CONCLUSIONS

Roughness and density measurements of films of PHS as a function of film thickness were studied using X-ray reflectivity. No changes in the values for these variables within error limits were found in the 50 nm to 250 nm range, suggesting that the resulting topography of those films after spin coating averaged through the resist surface is not susceptible to changes in the polymer mass fraction in solution (3%-10%), when a single-component resist formulation is evaluated. A series of neutron and X-ray reflectivity experiments were used to monitor the moisture uptake in PHS films as a function of film thickness. Primarily we reveal that moisture is absorbed uniformly throughout the film, without preferential absorption at the interface regardless of whether the substrate is hydrophilic or hydrophobic. We also observe that the initial moisture uptake for the film is non-reversible. Ignoring the initial uptake, the degree of swelling (thickness) observed with both X-rays and neutrons are similar, on the order of 3% to 4%. There are strong *suggestions* that the moisture-induced increase in the overall film (swollen film) density decreases with film thickness, but confirmation of this notion is beyond our current resolution. Additional experimentation would be required to confirm this possibility.

## 5. ACKNOWLEDGMENTS

The authors thank S. K. Satija and J. L. Lenhart for useful discussions and their assistance during these measurements. The authors also gratefully acknowledge DARPA for financial support under contract N66001-00-C-8803.

## 6. REFERENCES

---

1. W.E.Wallace, J.H.van Zanten and W-L.Wu. *Phys.Rev E* **52** (1995) R3329.
2. W.J.Orts, J.H.van Zanten W-L.Wu and S.K.Satija. *Phys.Rev.Lett.* **71** (1993) 867.
3. J.H.van Zanten, W.E.Wallace and W-L.Wu. *Phys.Rev E* **53** (1996) R2053
4. W-L.Wu , J.H.van Zanten and W.J.Orts. *Macromol.* **28** (1995) 771.
5. G.Reiter. *Macromol.* **27** (1994) 3096.
6. E.K.Lin, W-L.Wu and S.K.Satija. *Macromol.* **30** (1997) 7224.
7. A.Karim, G.P.Felcher and T.P.Rusell. *Macromol.* **27** (1994) 6973.
8. W-L. Wu, W.J.Orts, C.J.Majkrzak and D.L.Hunston. *Pol. Eng. Sci.* **35** (1995) 1000.
9. E.K.Lin, R.Kolb, S.K.Satija and W-L.Wu. *Macromol.* **32** (1999) 3753.
10. W-L.Wu, W.E.Wallace, E.K.Lin, G.W.Lynn, C.J.Glynka, E.T.Ryan and H-M.Ho. *J.Appl.Phys.* **87** (2000) 1193.
11. E.K.Lin, W-L.Wu, C.Jin and J.T.Wetzel. *Mat.Res.Soc.Symp.Proc.* **612** (2000) D4.1.1.
12. U.Okoroanyanwu. *J. Vac. Sci. Technol.* **B18** (2000) 3381.
13. According to ISO 31-8, the term “molecular weight” has been replaced by “relative molecular mass,” symbol Mr. Thus, if this nomenclature and notation were to be followed in this publication, one would write Mr,n instead of the historically conventional Mn for the number average molecular weight, with similar changes for Mw, Mz, and Mv, and it would be called the “number average relative molecular mass.” The conventional notation, rather than the ISO notation has been employed for this publication.
14. Certain commercial equipment and materials are identified in this paper in order to specify adequately the experimental procedure. In no case does such identification imply recommendation by the National Institute of Standards and Technology nor does it imply that the material or equipment is necessarily the best available for this purpose.
15. All data in the manuscript, tables, and graphs are presented along with the standard uncertainty ( $\pm$ ) associated with the measurement.